Indian J Phys (March 2013) 87(3):223–228
DOI 10.1007/s12648-012-0207-y

ORIGINAL PAPER

Preparation and characterization of mixed iron–titanium oxide nanostructure

S H Mohamed[1,2]*, M El-Hagary[1,3] and A S Radwan[4]

[1]Physics Department, College of Science, Qassim University, P.O. Box 6644, Buryadh 51452, Saudi Arabia

[2]Physics Department, Faculty of Science, Sohag University, Sohag 82524, Egypt

[3]Physics Department, Faculty of Science, Helwan University, Helwan, Cairo 11792, Egypt

[4]Chemistry Department, College of Science, Qassim University, P.O. Box 6644, Buryadh 51452, Saudi Arabia

Received: 16 August 2012 / Accepted: 16 October 2012 / Published online: 18 November 2012

Abstract: The Fe_2O_3–TiO_2 mixed nanostructure was grown from Fe/Ti metallic source using evaporation–condensation method. The formation of mixed Fe_2O_3–TiO_2 nanostructures was confirmed by energy dispersive analysis of X-ray and X-ray diffraction analysis. The scanning electron microscopy showed that the samples consisted of large amounts of two kinds dispersed particulates. The small particulates had sizes in the range of 130–170 nm and the big particulates had sizes in the range of 300–800 nm. Optical properties including refractive index (n), extinction coefficient (k), energy band gap (E_g), and Urbach energy (E_u) of the mixed thin film were investigated by spectroscopic ellipsometer. The Fe_2O_3–TiO_2 nanostructure had low n values compared to the previously reported values for Fe_2O_3 and TiO_2, while the value of band gap (2.54 ± 0.02 eV) lied in between the band gap values of Fe_2O_3 and TiO_2. The mixed Fe_2O_3–TiO_2 nanostructures showed enhanced photocatalytic activities.

Keywords: Fe_2O_3–TiO_2 nanostructure; Optical properties; Photocatalysis

PACS Nos.: 81.15.Gh; 61.05.C-; 78.66.-w

1. Introduction

Nanostructured materials have drawn a great deal of interest due to their unique properties and potential applications in many technologies, including nanoelectronics, biotechnology, energy storage, and conversion [1–12]. The iron oxide is a widely investigated material as a result of its various applications in biomedical [13], magnetic recording [14], wastewater treatment [15], Li-ion battery [16], field effect transistors [17], gas sensors [18], etc.

Titanium dioxide (TiO_2) is also widely used for optical and electrical applications because of its low cost and interesting properties such as high refractive index and high dielectric constant. The unique chemical, optical, and electronic properties of TiO_2 make it viable for several applications pertaining to photocatalysts [19–21], gas sensors [12], optical devices [22], solar cells [23], etc.

In order to bring together the beneficial properties of Fe_2O_3 and TiO_2, the nanocomposite of the mixture of these two semi-conducting oxides were prepared by evaporation–condensation method. The crystal growth and morphology characteristics were investigated. The optical constants were evaluated via spectroscopic ellipsometer (SE) measurements. The photocatalytic activities were studied using artificial light for the degradation of methylene blue (MB).

2. Experimental details

The Fe_2O_3–TiO_2 nanostructure was grown using evaporation–condensation method. The synthesis process was carried out in a controllable horizontal tube furnace with an alumina on Pt coated ($\sim$25 to 30 nm) Si (100) wafers and quartz substrates (cut into 1×1 cm and ultrasonically

*Corresponding author, E-mail: abo_95@yahoo.com

cleaned). The Pt coating of Si and quartz substrates was done using AC Ion sputtering device (JFC-1100E). The Fe_2O_3–TiO_2 nanostructures were prepared using a mixture of Ti (99.98 %)/Fe (99.999 %) with 50 wt% each. The Ti/Fe metal was placed in an alumina boat positioned at the center of the heating zone of the furnace. The Pt coated Si and quartz substrates were put after 1 cm and up to 10 cm distance from the alumina boat. A mixture of flowing Ar with 200 sccm (standard cubic centimeter per minute) and O_2 with 1.3 sccm was introduced into the alumina tube. Concurrently the temperature was raised rapidly up to 700 °C, and then it was raised with a heating rate of 3 °C/min up to 1,150 °C and kept for 30–90 min. After that, the furnace was cooled down to room temperature.

The surface morphology and crystal structure of the synthesized nanostructures were investigated by scanning electron microscope (SEM) (JOEL, model JSM-6380 LA) and X-ray diffraction (XRD) (Shimadzu Diffractometer XRD 6000) using Cu Kα_1 radiation ($\lambda = 1.54056$ Å). The chemical composition of the synthesized nanostructures was analyzed using energy dispersive analysis of X-ray (EDAX) unit attached with the SEM. The SEM and EDAX measurements were carried out for samples prepared on Si (100) and the XRD measurements were carried out on quartz substrates.

The optical data for Fe_2O_3–TiO_2 nanostructured films were acquired using a PHE-102 variable angle spectroscopic ellipsometer (Angstrom Advanced Inc.) in the wavelength range 350–1,100 nm (energy range 3.54–1.13 eV). The measurements were carried out on samples prepared on Si(100) substrates. The data were acquired at angles of incidence of 60°, 65°, and 70°. The instrument measured the complex ratio of the Fresnel reflection coefficients for *p*-and *s*-polarized light and gave the ratio in terms of the ellipsometric parameters ψ and Δ defined by the equation

$$F = \tan(\Psi)\exp(i\Delta) = \frac{\tilde{r}_p}{\tilde{r}_s} \quad (1)$$

where $\tilde{r}_p$ and $\tilde{r}_s$ are the amplitude reflection coefficient for light polarized in the *p*-and *s*-plane of incidence, respectively. The data obtained from the ellipsometer were accurately modeled using the PHE-102 software package. Ellipsometric data ψ and Δ for variable wavelengths were fitted to the optical model.

The photocatalytic behavior of the synthesized nanostructures was mainly tested by measuring the decomposition of methylene blue ($C_{16}H_{18}ClN_3S{\cdot}xH_2O$). A sample, on Si(100) substrate, with size of 1 × 1 cm^2 was added to 10 ml of dye solution, with a concentration of 1 mmol/l, in a small beaker. A commercial UV lamp with a wavelength centered at 254 nm was used for UV irradiation. Before irradiation, the samples were put in the dark for 10 min to ensure stable adsorption. After desired time intervals, the concentration of the solution was analyzed by recording the characteristic absorption of MB (682 nm) by a UV–visible spectrophotometer (JASCO).

3. Results and discussion

XRD pattern of mixed Fe_2O_3–TiO_2 nanostructure is shown in Fig. 1. The pattern can be mainly indexed as a mixture of cubic Fe_2O_3 (JCPDS card file no: 39-1346) and monoclinic β-TiO_2 (JCPDS file no: 46-1238). The peak around 21.2° could not be indexed to either Fe_2O_3 or β-TiO_2. However, it may be indexed to $Fe_2Ti_3O_9$ (JCPDS file no: 40-0850). The formation of $Fe_2Ti_3O_9$ phase could be explained by the fact that at high temperature, certain percentage of the Fe^{3+} ions present at the surface of TiO_2, diffused into the bulk TiO_2 producing a substitutional solid solution, in which Fe^{3+} is dispersed in the lattice of TiO_2. In fact, as the Fe^{3+} radius is similar to that of Ti^{4+}, the substitution of iron in the matrix of TiO_2 is a favorable process [24].

The formation of mixed Fe_2O_3–TiO_2 is also confirmed by EDAX as shown in Fig. 2. The atomic percentages of Ti, Fe, and O are found to be 20.5, 15.79, and 63.71 at%, respectively.

Figure 3 shows SEM image with low and high magnifications of mixed Fe_2O_3–TiO_2 nanostructure. The SEM image shows that the sample consists of large amounts of two kinds dispersed particulates. The small particulates have sizes in the range of 130–170 nm and the big particulates have sizes in the range of 300–800 nm. The presence of two kinds of particulates may be related to the presence of different crystalline phases as revealed by XRD.

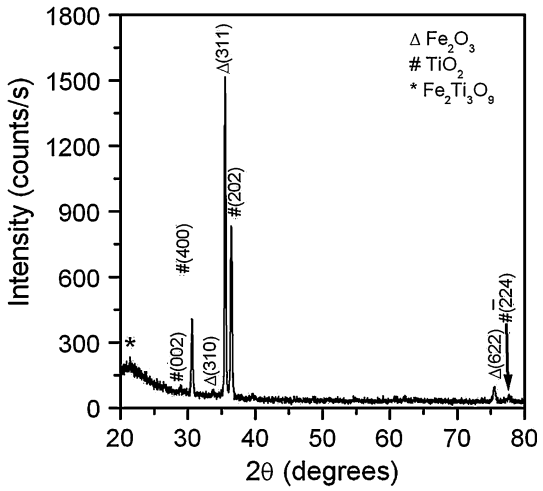

Fig. 1 XRD patterns of mixed Fe_2O_3–TiO_2 nanostructure

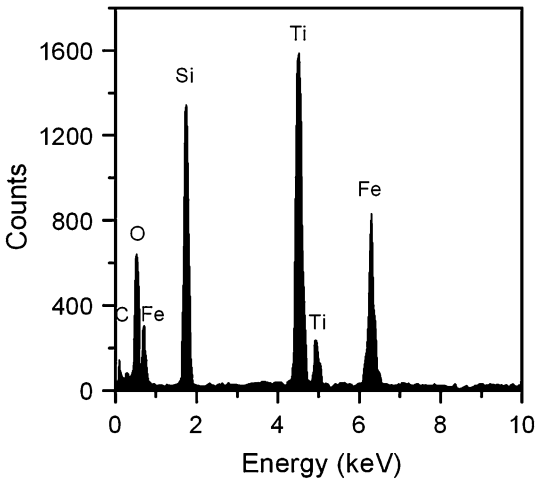

Fig. 2 EDAX spectra of Fe_2O_3–TiO_2 nanostructure

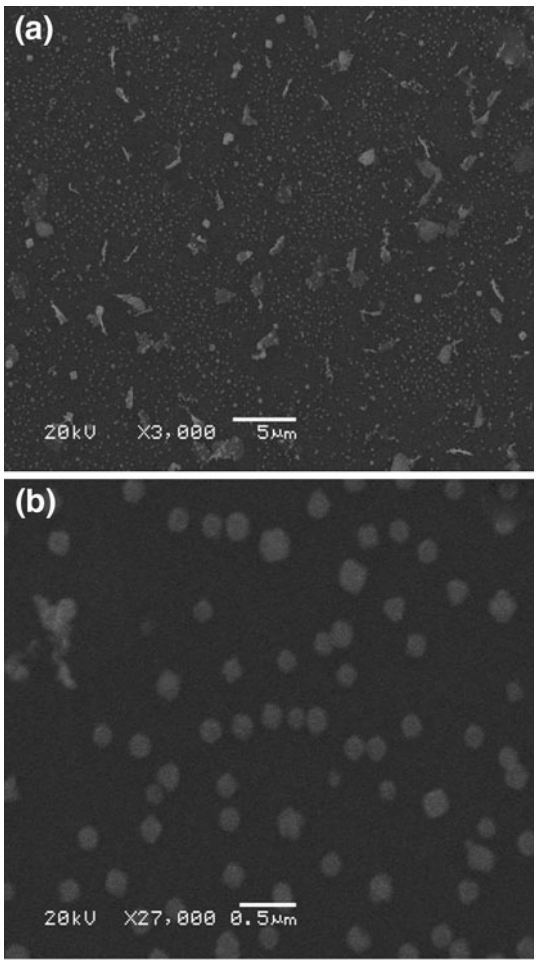

Fig. 3 (**a**) Low and (**b**) high magnifications SEM images of Fe_2O_3–TiO_2 nanostructure

Based on the film characterization by variable angle spectroscopic ellipsometer (VASE), the as-deposited nanostructure films are initially represented by one-layer model with only a dense Fe_2O_3–TiO_2 layer but the fitting was not good. The physical model of the film can only be represented by a two-layer model with an additional surface roughness layer (SRL) of mixed film material and voids. The use of more complicated layer models does not significantly improve the fit. The thickness of the surface layer was strongly correlated to the thickness of the main layer. The optical constants of Si obtained by Herzinger et al. [25] were used for the substrate. The complex refractive index of the SRL was calculated by the Bruggeman effective medium approximation (BEMA) assuming a mixture of the "Cauchy-material" and a fitted percentage (volume fraction) of voids (air). The complex refractive index of the film was described by Lorentz oscillator model. From a Lorentz oscillator model, the complex dielectric function can be expressed by the following relation [26]:

$$\varepsilon(h\nu) = \varepsilon_\infty + \sum_{j=1}^{N} \frac{A_j}{E_j^2 - (h\nu)^2 - iB_j h\nu} \tag{2}$$

where A_j is the amplitude, E_j is the center energy of jth oscillator, B_j is the broadening of each oscillator, hν is the photon energy in eV and ε_∞ is high dielectric constant. The four terms (ε_∞, A_j, E_j, and B_j) were used as fit parameters. The thickness and the voids fraction of the BEMA surface layer and the thickness of the interface layer were also selected as fit parameters.

An example for the best fit of the experimental Δ and Ψ of the Fe_2O_3–TiO_2 nanostructure film is shown in Fig. 4(a) and 4(b). It is seen that there is a good agreement between the simulated and the measured data. Thus, the optical constants can be adequately extracted. The thickness of the layers (film/surface roughness), the voids fraction and the mean square error (expressing the quality of the fits; MSE) determined by VASE data fits are summarized in Table 1.

Figure 5(a) and 5(b) show, respectively, the results of the ellipsometric analysis for refractive index (n) and extinction coefficient (k), as a function of wavelength. One can see that the refractive index first increases with the wavelength up to 406 nm and then decreases normally with wavelength. The variation of refractive index is similar to that of polycrystalline Fe:TiO_2 films prepared on indium tin oxide glass substrate by using sol–gel technique [27]. It is also observed that the magnitude of n at $\lambda = 550$ nm (1.59) is much lower than values 2.52 and 2.75 reported for anatase and rutile TiO_2, respectively [28] and also lower than the reported value (2.2 eV) of bulk α-Fe_2O_3 [29]. This may be attributed to the low packing density observed for the films obtained by the used CVD technique [30]. The

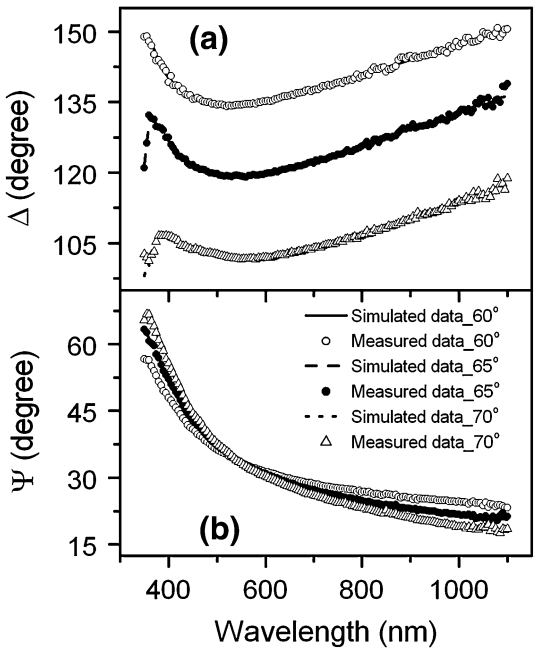

Fig. 4 (**a**) Measured and calculated Δ spectra at 65° and 70° angles of incidence for Fe_2O_3–TiO_2 nanostructure. (**b**) The same for ψ

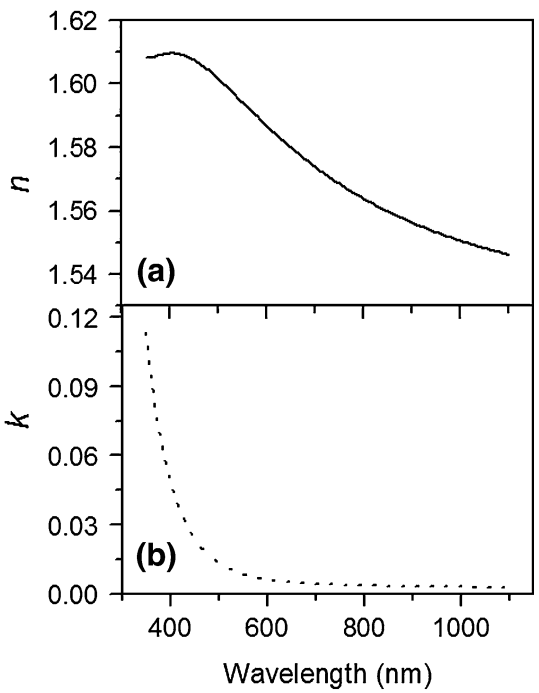

Fig. 5 (**a**) The refractive index and (**b**) extinction coefficient of Fe_2O_3–TiO_2 nanostructure

Table 1 Thickness derived from the ellipsometric data fitting (film/surface roughness), voids fraction, the mean square error (MSE), refractive index at 550 nm, optical band gap (E_g), and Urbach energy

Thickness (nm) (film/surface roughness)	Voids fraction %	MSE	*n* (at 550 nm)	Eu (neV)	E_g (eV)
93.5/3.1	64.3	1.1	1.59	418	2.54 ± 0.02

k values decrease with increasing wavelength and became close to zero at higher wavelengths.

The absorption coefficient (α) was calculated using the obtained *k* values from the relation:

$$\alpha = \frac{4\pi k}{\lambda} \tag{3}$$

For crystalline TiO_2 and Fe_2O_3, optical transitions have been shown to be direct [31, 32] as well as indirect [33, 34]. The variation in the absorption coefficient as a function of photon energy is shown in Fig. 6(a) and was fitted to allowed indirect transitions given by

$$(\alpha h\nu) = A\left(h\nu - E_g\right)^2 \tag{4}$$

where A is a constant, h is Planck's constant, ν is the frequency, and E_g is the band gap energy. A plot of $(\alpha h\nu)^{1/2}$ versus hν is shown in Fig. 6(b). The E_g value is obtained by extrapolating the linear part to intercept with the energy axis and is found to be 2.54 ± 0.02 eV. This value is lower than the values 3.2 and 3.02 eV reported for anatase and rutile TiO_2 [35], respectively, while it is higher than the values 1.71–2.13 eV reported for Fe_2O_3 [32, 34].

To evaluate the near band gap edge characteristics of the Fe_2O_3–TiO_2 nanostructures, the absorption behavior at lower photon energy can be interpreted by the Urbach rule:

$$\alpha = K\exp(E/E_u) \tag{5}$$

where K is constant and E_u is Urbach energy which is interpreted as the width of the tails of localized states in the band gap [36, 37]. The absorption in this region is due to transitions between extended states in one band and localized states in the exponential tail of the other band as well as the effects of all defects [38]. The value of E_u was calculated from Fig. 6(a). The obtained value of E_u is 418 meV. The obtained value of E_u for Fe_2O_3–TiO_2 nanostructure is lower than the value 713 meV obtained for TiO_2 synthesized by co-precipitation method [39]. It suggests that the defects in the Fe_2O_3–TiO_2 depend mainly on the preparation conditions used in the CVD or the PVD method and not on the method itself.

The UV–Vis absorbance spectra and the degradation rate curve of MB change with reaction time are shown in Fig. 7(a) and 7(b), respectively. The main peaks of MB at 668 and 395 nm degraded flatly under UV irradiation. The decomposition of the MB increases as the irradiation time increases. The obtained degradation curve is better than the highly doped TiO_2 films reported in [40, 41]. The excellent

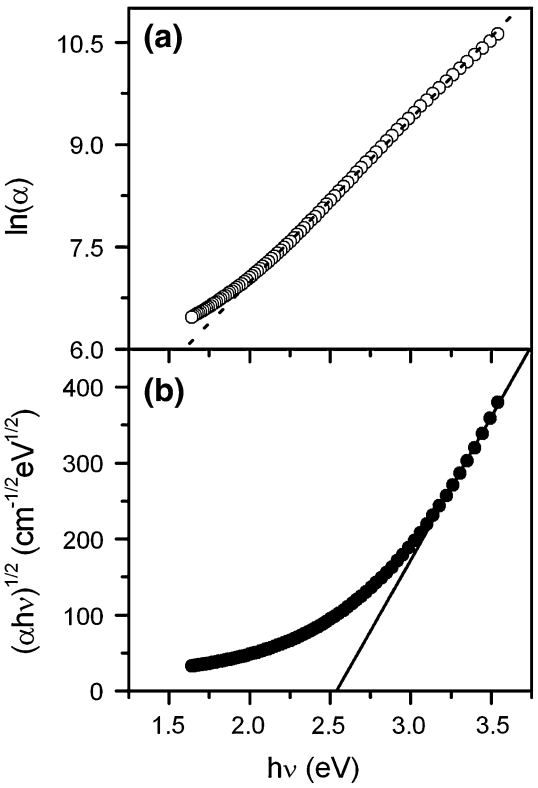

Fig. 6 (**a**) Plot of lnα as a function of energy and (**b**) typical best fit of $(\alpha h\nu)^{1/2}$ versus photon energy (hν)

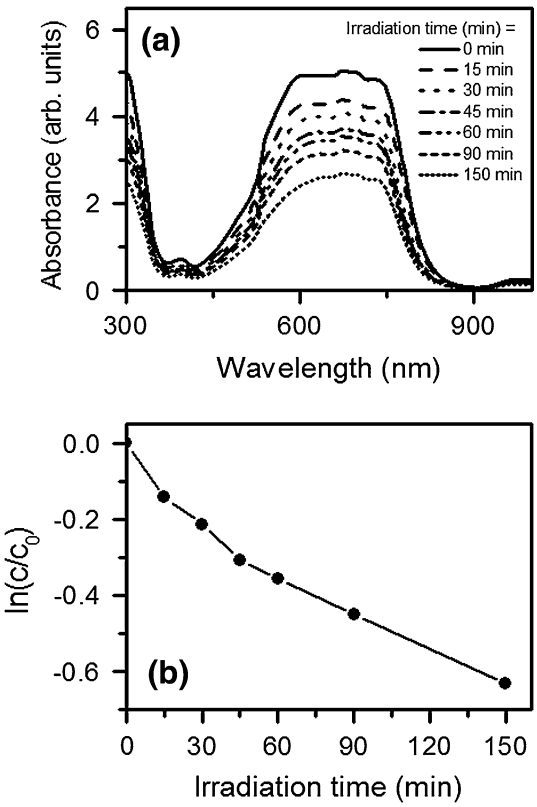

Fig. 7 (**a**) UV–Vis absorbance spectra and (**b**) the degradation rate curve of MB change with reaction time

photocatalytic degradation is due to the following reasons: (i) the ions of Fe^{3+} can enhance the intensity of absorption in the UV–Vis light region and make a red shift in the band gap transition of the Fe_2O_3–TiO_2 nanostructure. So more photo-generated electrons and holes can be generated to accelerate photocatalytic reactions [42]. (ii) The large surface area and small particle size may be important factors in certain photocatalytic degradation reactions [43].

4. Conclusions

The TiO_2–Fe_2O_3 mixed nanostructure was prepared via vapor transport from Fe/Ti metallic source. XRD analysis revealed the presence of mixed phases of cubic Fe_2O_3, monoclinic β-TiO_2, and $Fe_2Ti_3O_9$. The formation of the mixed structure was also confirmed via EDAX. The optical constants were evaluated using spectroscopic ellipsometer and employing a two layer model. The refractive index of the prepared TiO_2–Fe_2O_3 nanostructure films at $\lambda = 550$ nm was 1.59 which is significantly lower than values for TiO_2 and Fe_2O_3. This was attributed to the low packing density observed for the films obtained by the used CVD technique. The optical band gap energy and the Urbach energy were calculated. The mixed Fe_2O_3–TiO_2 nanostructures showed enhanced photocatalytic activities. The obtained results may find applications in optoelectronics and degradation of organic wastes.

Acknowledgments This work is supported by the Deanship of Scientific Research at Qassim University under Contract No. 1646.

References

[1] S Sarmah and A Kumar *Indian J. Phys.* **84** 1211 (2010)
[2] F Shadman *Curr. Opin. Chem. Eng.* **1** 258 (2012)
[3] M Conte, PP Prosini and S Passerini *Mater. Sci. Eng. B* **108** 2 (2004)
[4] H-J Choi, S-M Jung, J-M Seo, D W Chang, L Dai and J-B Baek *Nano Energy* **1** 534 (2012)
[5] S Mitra, A Mandal, S Banerjee, A Dutta, S Bhattacharya, A Bose and D Chakravorty *Indian J. Phys.* **85** 649 (2011)
[6] G Mandal and T Ganguly *Indian J. Phys.* **85** 1229 (2011)
[7] S Sarmah and A Kumar *Indian J. Phys.* **85** 713 (2011)
[8] S Tekerek, A Kudret and Ü Alver *Indian J. Phys.* **85** 1469 (2011)
[9] S Karan, D Dutta Majumder and A Goswami *Indian J. Phys.* **86** 667 (2012)
[10] S Devi and M Srivastva *Indian J. Phys.* **84** 1561 (2010)
[11] J Bhadra and D Sarkar *Indian J. Phys.* **84** 693 (2010); J Bhadra and D Sarkar *Indian J. Phys.* **84** 1321 (2010)
[12] M R Vaezi, S K Shendy and T Ebadzadeh *Indian J. Phys.* **86** 9 (2012)
[13] J K Oh and J M Park *Prog. Polym. Sci.* **36** 168 (2011)

[14] Z Jing *Mater. Lett.* **60** 2217 (2006)
[15] P Xu et al *Sci. Total Environ.* **424** 1 (2012)
[16] C Wu, P Yin, X Zhu, C O Yang and Y Xie *J. Phys. Chem. B* **110** 17806 (2006)
[17] Z Fan, X Wen, S Yang and J G Lu *Appl. Phys. Lett.* **87** 013113 (2005)
[18] M Aronniemi, J Saino and J Lahtinen *Thin Solid Films* **516** 6110 (2008)
[19] M Andersson, L Osterlund, S Ljungstrom and A Palmqvist *J. Phys. Chem. B* **414** 338 (2002)
[20] Y-M Sung, J-K Lee and W-S Chae *Cryst. Growth Des.* **6** 805 (2006)
[21] Y-M Sung and J-K Lee *Cryst. Growth Des*. **4** 737 (2004)
[22] D Appell *Nature* **419** 553 (2002)
[23] N-G Park, J Van de Lagemaat and A J Frank *J. Phys. Chem. B* **104** 8989 (2000)
[24] X Zhang and L Lei *Appl. Surf. Sci*. **254** 2406 (2008)
[25] C M Herzinger, B Johs, W A McGahan, J A Woollam and W Paulson *J. Appl. Phys.* **83** 3323 (1998)
[26] R A Synowicki *Thin Solid Films* **313–314** 394 (1998)
[27] R Mechiakh, N Ben Sedrine and R Chtourou *Appl. Surf. Sci.* **257** 9103 (2011)
[28] D E Aspnes *J. Opt. Soc. Am.* **70** 1275 (1980)
[29] H Miyoshi and H Yoneyama *J. Chem. Soc. Faraday Trans.* **85** 1873 (1989)
[30] S H Mohamed, M El-Hagary and S Althoyaib *J. Alloys Compd.* **537** 291 (2012)
[31] H P Deshmukh, P S Shinde and P S Patil *Mater. Sci. Eng. B* **130** 220 (2006)
[32] A A Akl *Appl. Surf. Sci.* **233** 307 (2004)
[33] P S Shinde and C H Bhosale *J. Anal. Appl. Pyrolysis* **82** 83 (2008)
[34] M F Al-Kuhaili, M Saleem and S M A Durrani *J. Alloys Comp.* **521** 178 (2012)
[35] W Wunderlich, T Oekermann, L Miao, N T Hue, S Tanemura and M Tanemura *J. Ceram. Process. Res.* **4** 342 (2004)
[36] J C Tauc *Optical Properties of Solids* (Amsterdam: North-Holland) (1972)
[37] J C Tauc *Amorphous and Liquid Semiconductors* (New York: Plenum Press) (1974)
[38] V Srikant and D R Clarke *J. Appl. Phys.* **81** 6357 (1997)
[39] A Molea, V Popescu and N A Rowson *Powder Technol.* **230** 203 (2012)
[40] S H Mohamed and E R Shaaban *Physica B* **406** 4327 (2011)
[41] S H Mohamed, M El-Hagary and S Althoyaib *Eur. Phys. J. Appl. Phys.* **57** 20301 (2012)
[42] S Zhan et al *J. Colloid. Interf. Sci.* **355** 328 (2011)
[43] M H Zhou, J G Yu, B Chen *J. Hazard. Mater. B* **137** 1838 (2006)